BRAIN
ORIGINAL ARTICLE

Biallelic mutations in *RNF220* cause laminopathies featuring leukodystrophy, ataxia and deafness

Antonella Sferra,[1] Paola Fortugno,[2,3] Marialetizia Motta,[1] Chiara Aiello,[1] Stefania Petrini,[4] Andrea Ciolfi,[1] Francesca Cipressa,[5] Isabella Moroni,[6] Vincenzo Leuzzi,[7] Luisa Pieroni,[8] Federica Marini,[9,10] Odile Boespflug Tanguy,[11,12] Eleonore Eymard-Pierre,[13] Federica Rachele Danti,[6] Claudia Compagnucci,[1] Giovanna Zambruno,[1] Alfredo Brusco,[14] Filippo M. Santorelli,[15] Luisa Chiapparini,[16] Paola Francalanci,[17] Anna Livia Loizzo,[18] Marco Tartaglia,[1] Gianluca Cestra[5,8,19,†] and Enrico Bertini[1,†]

†These authors contributed equally to this work.

Leukodystrophies are a heterogeneous group of rare inherited disorders that mostly involve the white matter of the CNS. These conditions are characterized by primary glial cell and myelin sheath pathology of variable aetiology, which causes secondary axonal degeneration, generally emerging with disease progression.

Whole exome sequencing performed in five large consanguineous nuclear families allowed us to identify homozygosity for two recurrent missense variants affecting highly conserved residues of *RNF220* as the causative event underlying a novel form of leukodystrophy with ataxia and sensorineural deafness.

We report these two homozygous missense variants (p.R363Q and p.R365Q) in the ubiquitin E3 ligase RNF220 as the underlying cause of this novel form of leukodystrophy with ataxia and sensorineural deafness that includes fibrotic cardiomyopathy and hepatopathy as associated features in seven consanguineous families. Mass spectrometry analysis identified lamin B1 as the RNF220 binding protein and co-immunoprecipitation experiments demonstrated reduced binding of both RNF220 mutants to lamin B1. We demonstrate that *RNF220* silencing in *Drosophila melanogaster* specifically affects proper localization of lamin Dm0, the fly lamin B1 orthologue, promotes its aggregation and causes a neurodegenerative phenotype, strongly supporting the functional link between RNF220 and lamin B1. Finally, we demonstrate that RNF220 plays a crucial role in the maintenance of nuclear morphology; mutations in primary skin fibroblasts determine nuclear abnormalities such as blebs, herniations and invaginations, which are typically observed in cells of patients affected by laminopathies.

Overall, our data identify *RNF220* as a gene implicated in leukodystrophy with ataxia and sensorineural deafness and document a critical role of RNF220 in the regulation of nuclear lamina. Our findings provide further evidence on the direct link between nuclear lamina dysfunction and neurodegeneration.

1 Genetics and Rare Diseases Research Division, Bambino Gesù Children's Hospital, IRCCS, 00146 Rome, Italy
2 Department of Life, Health and Environmental Sciences University of L'Aquila, 00167 Rome, Italy
3 Human Functional Genomics, IRCCS San Raffaele Pisana, 00166 Rome, Italy
4 Confocal Microscopy Core Facility, Research Laboratories, Ospedale Pediatrico Bambino Gesù, 00146 Rome, Italy
5 University of Rome "Sapienza", Department of Biology and Biotechnology, 00185 Rome, Italy

6 Department of Pediatric Neuroscience, Fondazione IRCCS Istituto Neurologico Carlo Besta, 20133 Milan, Italy
7 Department of Human Neuroscience, Unit of Child Neurology and Psychiatry, Sapienza University, 00185 Rome, Italy
8 Santa Lucia IRCCS Foundation, 00179 Rome, Italy
9 Institute of Biochemistry and Clinical Biochemistry, Università Cattolica del Sacro Cuore, 00168 Rome, Italy
10 Department of Laboratory Diagnostic and Infectious Diseases, Fondazione Policlinico Universitario Agostino Gemelli IRCCS, 00168 Rome, Italy
11 Service de Neurologie Pédiatrique, Centre de reference leucodystrophies et leucoencephalopathies de cause rare (LEUKOFRANCE), APHP Hopital Robert-Debré, 75019 Paris, France
12 Université de Paris, NeuroDiderot, UMR 1141 INSERM 75651 Paris, France
13 Service de Cytogénétique Médicale CHU de Clermont Ferrand, Hopital ESTAING 63003 Clermont Ferrand, France
14 Department of Medical Sciences, University of Torino, 10124 Turin, Italy
15 Molecular Medicine, IRCCS Stella Maris Foundation, 56128 Pisa, Italy
16 Neuroradiology Department, Fondazione IRCCS Istituto Neurologico Carlo Besta, 20133 Milan, Italy
17 Department of Laboratories, Pathology Unit, IRCCS Bambino Gesù Children's Hospital, 00165 Rome, Italy
18 DIDASCO Società Cooperativa Sociale- Centro di riabilitazione, 00185 Rome, Italy
19 Institute of Molecular Biology and Pathology (IBPM), National Research Council (CNR), 00185 Rome, Italy

Correspondence to: Enrico Bertini
Unit of Neuromuscular and Neurodegenerative Disorders
Genetics and Rare Diseases Research Division
Bambino Gesù Children's Hospital, IRCCS, V.le S. Paolo
15, 00146 Rome, Italy
E-mail: bertini@opbg.net

Correspondence may also be addressed to: Antonella Sferra
E-mail: antonella.sferra@opbg.net

Introduction

Leukodystrophies are a group of neurodegenerative diseases that result from inherited defects in myelin sheath formation and/or maintenance in pyramidal and cerebellar neurons.[1,2] They represent an important cause of progressive neurological disability in young patients. Although many forms have recognizable genetic, imaging and metabolic patterns, there are still cases running in families with unsolved aetiology.[3]

We report on a novel form of autosomal recessive leukodystrophy identified in seven nuclear families characterized by progressive ataxia and deafness (AR-LAD) combined with fibrotic cardiomyopathy and hepatopathy as major associated features.

Whole exome sequencing performed in five large consanguineous nuclear families allowed us to identify homozygosity for two recurrent missense variants affecting highly conserved residues of RNF220 as the causative event underlying AR-LAD.

RNF220 encodes an evolutionarily conserved RING finger E3 ubiquitin ligase[4] highly expressed in the developing nervous system, where it modulates both ventral spinal cord patterning,[5–7] and in cerebellum development.[8] According to its neuronal expression, RNF220 has recently been involved in the regulation of neural stem cell proliferation and differentiation[9] and in the development of noradrenergic neurons.[10]

In this study, we demonstrate that the RNF220 protein, which is mutated in the novel syndromic leukodystrophy AR-LAD, binds lamin B1 and plays a crucial role in the maintenance of nuclear integrity by regulating nuclear laminar proteins. Interestingly, this form of hypomyelinating leukodystrophy recalls, for some aspects, the adult-onset autosomal dominant leukodystrophy (ADLD) caused by either genomic duplications encompassing the lamin B1 gene (LMNB1) or deletions upstream of this gene. LMNB1 encodes one of the major components of the nuclear lamina, and all ADLD-related mutations result in increased lamin B1 protein levels in the brain tissue of affected individuals.[11,12]

Overall, our findings provide new insights into RNF220 nuclear functions and its involvement in AR-LAD pathogenesis and corroborate the implication of nuclear lamina defects in the pathogenesis of brain white matter disorders.

Materials and methods

Standard protocol approvals, registrations, and patient consent

The study was approved by the Ethical Committees of the Children Hospital Bambino Gesù, Rome, Italy, in agreement with the Declaration of Helsinki. Informed consent was signed by the parents of the patients.

Whole exome sequencing and proteomic analysis

Detailed methods of the whole exome sequencing and proteomic analysis are described in the Supplementary material.

Cell culture

COS-1, HEK-293T and human primary skin fibroblasts were grown in Dulbecco's modified Eagle medium (high glucose formulation) supplemented with 10% foetal bovine serum (Thermo Fisher Scientific), 2 mM L-glutamine and 1% penicillin-streptomycin antibiotic at 37°C in a 5% CO_2 humidified atmosphere. Induced pluripotent stem cells (iPSCs) were purchased from the Coriell Institute (Cod GM23338, GM23340). The iPSCs were derived from human fibroblasts and reprogrammed using episomal technology. The iPSCs were differentiated into motor neurons as previously described.[13]

Plasmid constructs

To generate RNF220 constructs, the entire cDNA sequence (NM-018150) was amplified from the cDNA clone MGC39525 (Thermo Scientific) and inserted into a pFLAG-CMW-6a vector. RNF220 mutants were generated by site-directed mutagenesis using the QuikChange-XLII Site-Directed Mutagenesis kit (Stratagene) according to the manufacturer's instructions. All constructs were confirmed by DNA sequencing.

Cell transfection

Transient transfection of COS-1 and HEK-293 cells was achieved by using Lipofectamine 2000 reagent according to the manufacturer's instructions (Thermo Fisher Scientific). Forty-eight hours after transfection, cells were fixed or recovered for protein extraction.

Preparation of nuclear extracts and co-immunoprecipitation experiments

Preparation of nuclear extracts from transiently or mock transfected HEK-293T cells was performed as previously described.[14] A 400 μg sample of nuclear extract was incubated with 30 μl of anti-FLAG M2 antibody covalently bound to agarose beads at 4°C for 1 h, while being rocked gently. After incubation, samples were centrifuged to form pellet FLAG resins. After extensive washing, retained proteins were resuspended in 30 μl of Laemmli buffer, separated using SDS-PAGE and analysed by western blotting.

Immunohistochemistry

CD1 mouse brain slices were fixed in 4% paraformaldehyde at 4°C for 20 min, permeabilized in PBS-0.15% Triton™ X-100 (Sigma), blocked for 1 h in PBS-5% bovine serum albumin (BSA) (Sigma) and incubated with primary antibodies at 4°C overnight. Primary antibodies were diluted in PBS-1% BSA according to the following dilutions: rabbit anti-RNF220 (1:50, Sigma), mouse anti-Smi32 (1:500, Sigma), mouse anti-calbindin (1:500, Sigma) and mouse anti-GFAP (1:500, BD Biosciences). Slices were washed three times in PBS and incubated with Alexa Fluor-conjugated secondary antibodies (Thermo Fisher Scientific) for 1 h at room temperature, and nuclei were counterstained with Hoechst (Sigma).

Immunocytochemistry

Fibroblasts were seeded in 24-well cluster plates onto 12 mm cover glasses. After 24 h of culture in complete medium, cells were fixed with ice-cold methanol for 7 min, blocked with PBS-5% BSA (Sigma) for 1 h and subsequently incubated with the indicated primary antibodies at 4°C overnight. Primary antibodies were diluted in PBS-1% BSA according to the following dilutions: mouse anti-lamin AC (1:50, Santa Cruz), rabbit anti-lamin B1 (1:500, Abcam) and mouse anti-nesprin-1 (MANNES1A-7A12) (1:50, Thermo Fisher Scientific).[15] Cells were washed three times in PBS and incubated with Alexa Fluor-conjugated secondary antibodies (Thermo Fisher Scientific) for 1 h at room temperature. Nuclei were counterstained with Hoechst (Sigma).

COS-1 cells transiently transfected were fixed in 4% paraformaldehyde for 15 min, blocked with PBS-5% BSA (Sigma) for 1 h and subsequently incubated with the primary mouse anti FLAG antibody (1:500, Sigma) for 1 h at room temperature or with the indicated primary antibodies at 4°C overnight: rabbit anti-20S proteasome (1:100, Thermo Fisher Scientific) and rabbit anti-ASF/SF2 (1:100, Abcam). Cells were washed three times in PBS and incubated with Alexa Fluor-conjugated secondary antibodies (Thermo Fisher Scientific) for 1 h at room temperature. Nuclei were Hoechst (Sigma) counterstained.

Confocal microscopy analysis

Confocal imaging was performed on an Olympus FluoView FV1000 confocal microscope equipped with Multi Ar (458–488 and 515 nm), 2× He/Ne (543 and 633 nm) and 405-nm diode lasers. Sequential confocal images were acquired using a HC PLAPO CS2 40× oil-immersion objective with a 1024 × 1024 format, 400 Hz scan speed and a z-step size of 0.4 μm. The lasers' power, beam splitters, filter settings, pinhole diameter and scan mode were the same for all examined samples of each staining. The spatial relationship between RNF220 and 20S proteasome was quantified by co-localization analysis module of LAS X Leica software, using Manders' overlap coefficient (OC). Its value can range from 0 to 1, where 0 represents a total exclusion, 0.5 a random overlap, and 1 reflects 100% co-localization between both images. The co-localization was considered significant when OC > 0.5.

Drosophila strains and crosses

Fly stocks were maintained on *Drosophila* standard medium (Nutri-Fly® Genesee Scientific) at 25°C and crosses were performed at 18 and 25°C. RNF220 downregulation in different tissues was obtained by crossing UAS RNF220 RNAi (BDSC 61303) with Eyeless-GAL4 (eye imaginal disc and larval salivary glands), GMR-GAL4 (adult eye) or Mef2-GAL4 (larval muscles) flies. All stocks were provided by the Bloomington Stock Center and are described in flybase.org.

Drosophila salivary glands immunostaining

Third instar larval salivary glands were dissected in 0.7% NaCl, transferred in 1.8% formaldehyde and 40% acetic acid on a coverslip, gently squashed and immediately frozen in liquid nitrogen. After flipping off the coverslip, slides were immersed in ice cold Tris-buffered saline (TBS) for 10 min and permeabilized for 20 min in TBS-Triton 1%. Slides were then incubated with anti-lamin Dm0 (1:10; ADL67.10-S Developmental Studies Hybridoma Bank) and anti-lamin C (1:10; LC28.26-S Developmental Studies Hybridoma Bank) antibodies overnight at 4°C in a wet chamber. Salivary gland preparations were washed for 10 min with TBS-Triton 0.05% and incubated with anti-mouse TRITC (Jackson Immuno Research) for 1 h at room temperature. After two washes with TBS-Triton 0.05%, slides were mounted in VECTASHIELD Antifade Mounting Medium with DAPI (Vector) to stain DNA. Intact polytene chromosomes nuclei were analysed using a Zeiss AxioPlan epifluorescence microscope (Carl Zeiss) equipped with a cooled CCD camera (Photometrics). Images were pseudocoloured and merged with Adobe Photoshop CS4.

RNA extraction, cDNA synthesis, real-time PCR and PCR

Total RNA from UAS-RNF220-RNAi/Mef2 GAL4 and control +/Mef2 GAL4 was extracted from third instar larvae (two larvae/sample)

using NucleoZOL (Macherey Nagel) by following the manufacturer's manual, and genomic DNA was digested with Invitrogen™ Dnase I Amplification Grade (Thermo Fisher Scientific). A sample of each total RNA (400 ng) was retrotranscribed into equal amounts of cDNA using the iScript™ cDNA Synthesis kit (Bio-Rad) and 35 ng of cDNA for each reaction were amplified by quantitative real-time PCR (RT-qPCR) using SsoAdvanced™ Universal SYBR® Green Supermix kit (Bio-Rad) according to the manufacturer's protocol.

Total RNA from skin fibroblasts of patients and healthy individuals were isolated using the Total RNA Purification Plus kit (Norgen Biotek Corp) according to the manufacturer's protocol. Each RNA sample (500 ng) was reverse transcribed with the LunaScript® RT SuperMix kit (Euroclone) and 25 ng of cDNA for each reaction were amplified using RT-qPCR with Power SYBR® Green PCR Master Mix (Thermo Fisher Scientific).

RNF220 splice variants were amplified using 25 ng of cDNA obtained from skin fibroblasts of patients and healthy individuals and a commercial total human brain (Takara Bio) using the KAPA Taq PCR kit (Roche).

RNF220 mRNA expression levels in a commercially available human cDNA panels from healthy adult tissues (Takara Bio) and foetal brain areas (BioChain) was analysed by RT-qPCR using two inventoried TaqMan®-MBP probes (Thermo Fisher Scientific).

Data analysis and statistics

Results are presented as the mean ± standard error of the mean (SEM). The statistical analysis was performed using GRAPHPAD/Prism 7.0 software. Statistically significant differences between groups were analysed using the Student's t-test for normally distributed variables. Statistical significance was defined as *$P \leqslant 0.05$, **$P \leqslant 0.005$, ***$P \leqslant 0.0005$ and ****$P \leqslant 0.0001$.

Data availability

The raw liquid chromatography-mass spectrometry (LC-MS) data (e.g. mass spectra) have not been shared because they require specific software to be visualized, but are available upon request. The data that have been shared (Supplementary Table 3) are representative of raw data processing.

Results

Patients and genomic analyses

We used whole exome sequencing to study a trio from a consanguineous nuclear family of Roma ethnicity originating from Croatia (Family Pedigree 2) (Fig. 1A). In this family, three siblings were affected by a similar early-onset hypomyelinating leukodystrophy, having progressive ataxia, sensorineural deafness, fibrotic cardiomyopathy and hepatopathy as major associated features. Cardiac manifestations progressed to dilated cardiomyopathy that caused their deaths by the end of the first decade (Table 1 and Supplementary material). The proband Patient I, 3 had been enrolled in the 'Undiagnosed patients program', Ospedale Pediatrico, Bambino Gesù, Rome. Whole exome sequencing analysis excluded the occurrence of any functionally relevant variant(s) compatible with known Mendelian disorders based on the expected inheritance model and clinical presentation. Our variant filtering and prioritization strategy led us to identify eight genes carrying putative deleterious biallelic variants as the best candidates to underlie the trait (Supplementary Table 1). The following analysis, which took advantage of gnomAD's gene constraint metrics,[16] highlighted that RNF220 (MIM 616136) has by far the highest probability of being loss-of-function intolerant (pLI = 1, observed-to-expected ratio = 0.03–0.2). Moreover, bioinformatic analysis

showed that Arg365 is intolerant to missense variants [MetaDome's tolerance score (dn/ds) = 0.51; Supplementary Fig. 1[17]]. Overall, RNF220 [NM_018150.4:c.1094G>A, p.(R365Q)], with a CADD score of 25.8 was identified as the only putative candidate fitting the recessive transmission of the trait and homozygosity by descent. Co-segregation analysis confirmed homozygosity for the missense change in the other two affected siblings as well as heterozygosity in the two obligate carriers and in four healthy siblings. We also annotated this variant in population genetics databases, with a minor allele frequency < 0.01 (dbSNP: rs1010750511; maximum allele frequency in a gnomAD subpopulation = 0.0001202, with no homozygous individuals reported).

Three nuclear related families of a large consanguineous pedigree originating from southern Italy were identified to transmit a superimposed phenotype characterized by ataxia, deafness, hypomyelinating leukodystrophy and fatal cardiomyopathy, together with hepatopathy that was detected in the clinical follow-up.[18] Homozygosity mapping including the three AR-LAD-affected patients, six healthy siblings and four relatives (for pedigree, see Leuzzi et al.[18]) defined a likely region of homozygosity on chromosome 1p34.3-p33, encompassing the RNF220 gene. Based on the clinical overlap, a scan of the entire RNF220 coding sequence allowed us to identify a second missense change affecting an adjacent residue [c.1088G>A; p.(R363Q)] that co-segregated as a homozygous change with the trait. This mutation, c.1088G>A, with a CADD score of 32, was heterozygous in six additional healthy siblings and four relatives. It was annotated in the reference scientific databases with a minor allele frequency < 0.01 (dbSNP: rs780921270; maximum allele frequency in a gnomAD subpopulation = 0.000054 and no homozygotes reported, dn/ds = 0.54; Supplementary Fig. 1).

Finally, using Genematcher imputation, an additional seven affected subjects from three large Roma pedigrees (Fig. 1A) sharing an overlapping neurodegenerative disorder and homozygosity for the previously recognized c.1094G>A; (p.R365Q) substitution were identified. Interestingly, multiple sequence alignments performed with ClustalW showed that both missense variants, p.R363Q and p.R365Q, target evolutionarily conserved residues (Fig. 1B). Genotyping for single nucleotide polymorphisms opportunely selected within the homozygous genomic region encompassing RNF220 from affected and apparently unrelated Roma subjects (Pedigrees 2–4) showed a shared haplotype, indicating a founder effect (Supplementary Table 2).

The clinical features of the patients are schematically listed in Table 1, and their clinical reports are summarized in the Supplementary material (Case report). Most of the patients died during the follow up, and the main cause of death occurred after the appearance of a cardiomyopathy. Remarkably, all patients belonging to the Roma ethnicity harbouring the homozygous p.R365Q variant died around the end of the first decade, while patients originating from the southern Italian pedigree, carrying the homozygous p.R363Q, died by the end of the second decade.

Neuroimages showed a recognizable distribution of hypomyelination that diffusely involves the white matter of the brain and spares the white matter of the cerebellum (Fig. 2). Of note, the T_2 and FLAIR hyperintensity was particularly enhanced at the level of the periventricular anterior and posterior areas.

Histological analysis of the autopsy heart samples and liver biopsies from patients showed significant alterations (Supplementary Fig. 2). A heart sample from the autopsy of the 18-year-old Patient 3 in Pedigree 1[18] showed replacement of myofibres by fibrotic tissue associated with a prominent interstitial fibrosis (Supplementary Fig. 2A). Similarly, liver samples from an open biopsy of Patient I, 3 in Pedigree 2 (Fig. 1A) showed bridging

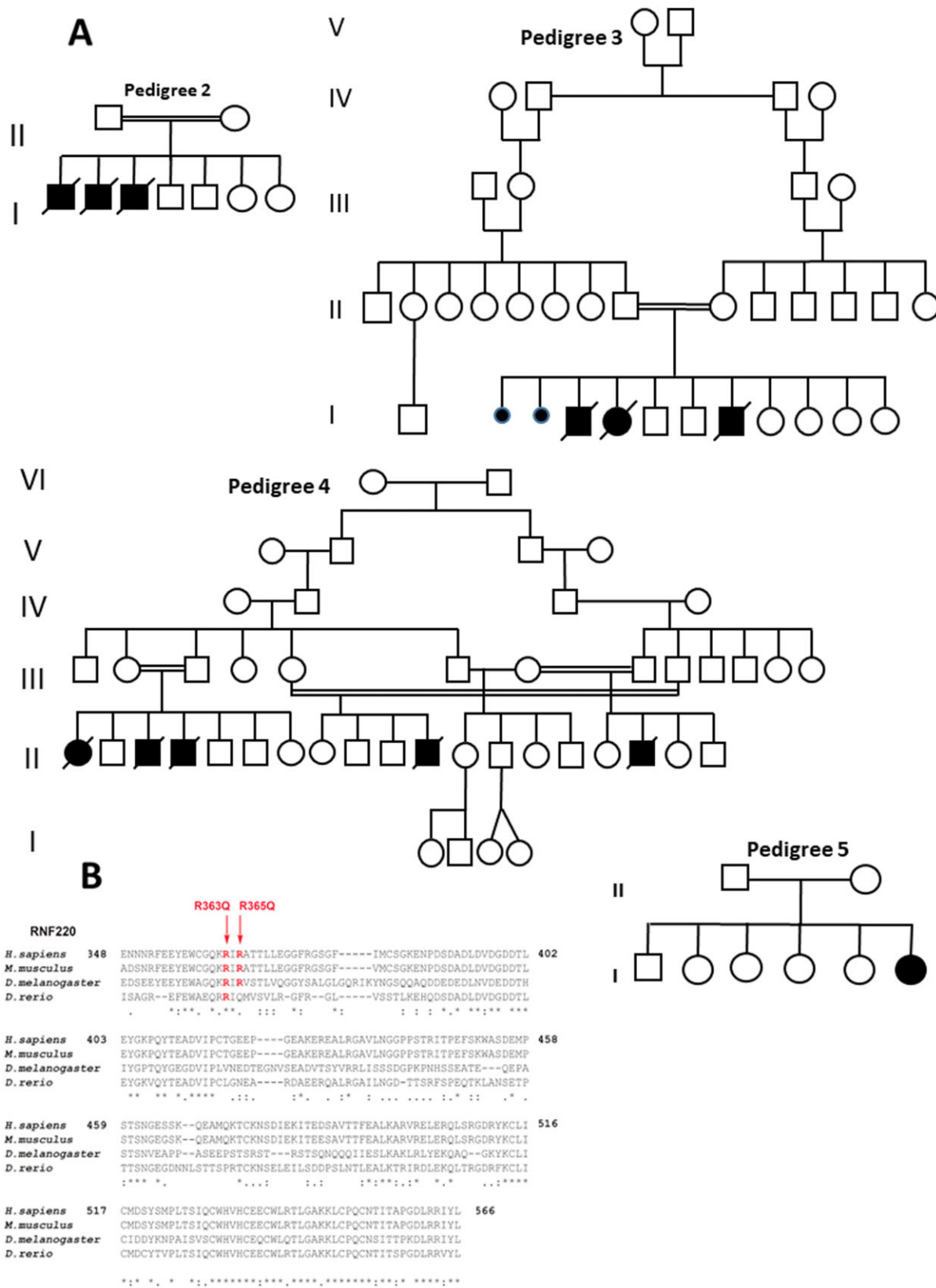**Figure 1 Pedigrees of the families and multiple sequence alignment of RNF220 proteins.** (A) Pedigree 1 was reported in Leuzzi *et al.*[18] (B) Multiple sequence alignment of RNF220 proteins (ClustalW) from different organisms around the sites affected by AR-LAD mutations R363Q and R365Q (in red). An asterisk indicates perfect conservation, a colon indicates strong similarity, and a full stop indicates weak similarity.

Table 1 Details of clinical features

Pedigree	Pedigree 1			Pedigree 2	Pedigree 3	Pedigree 4		Pedigree 5	
Patient	1[18]	2[18]	3[18]	1, 3	1, 4	II, 4	II, 11	II, 17	I, 6
Sex: age at death, y	F: 21	M: 18	F: 18	M: 10	M: 10	M: 10	M: 10	M: 11	F: 11
Ethnicity	Caucasian[a]	Caucasian[a]	Caucasian[a]	Roma	Roma	Roma	Roma	Roma	Roma
RNF220 mutation[b]	c.1088G>A p.Arg363Gly	c.1088G>A p.Arg363Gly	c.1088G>A p.Arg363Gly	c.1094G>A p.Arg365Gly	c.1094G>A p.Arg365Gly	c.1094G>A p.Arg365Gly	c.1094G>A p.Arg365Gly	c.1094G>A p.Arg365Gly	c.1094G>A p.Arg365Gly
Birth parameters[c]	3200 g[d] 25/50/50	3850 g[d] (75%ile) 50/75/50	3000 g[d] 25/50/50	3380 g[d] 50/50/50	2010 g[e] 3/3/3	3420 g[d] 50/	3200 g[f] 25/	3450 g[d] 50/	3120 g[g] 50/
Growth parameters[h]	7.3 y: 21 kg; 121 cm; 50.5 (25/50/50)	7 y: 27 kg; 130 cm; 57 (90/90/>98)	8 y: 52 kg (+3.05 SD); 137.4 cm (+1.2 SD); 9 y: ofc 55 cm (+1.67 SD)	5 mo: 61 cm[i]; 6.2 kg; 40 cm (<3%/<3%/<3%)	na	50/50 na	25/50 7.5 y (30/50/25)	50/50 na	50/50 7 y (50/50/50)
Consanguinity	+	+	+	+	+	+	+	+	−
First symptoms (age, y)	DD, mainly walking	DD, mainly walking	DD (mainly speech), mild ID	DD (mainly speech), ID	DD (walking and speech), ID	Ataxia (5)	Ataxia (5)	Ataxia (3), cognitive deterioration	Ataxia (4)
Neuropsychiatric manifestations									
Motor DD	+	+	+	+	+	−	−	−	−
ID (IQ)	−(78)	−(77)	+(59)	+	+(44)	−(85)	+	−	+(67)
Neurological manifestations									
Ataxia (age at dx, y)	+(3)	+(3)	+(1)	+(2)	+(2,5)	+(5)	+(5)	+(3)	+(4)
Spastic paraplegia (age)	+	+	+	+	+	+	+	+	+(10)
Hyperreflexia	+	+	+	+	+	+	+	+	+
Dysarthria	+	+	+	+	+	+	+	+	+
Peripheral neuropathy (axonal)	−	−	+	+	−	−	+	+	−
Seizures/EEG abnormalities	−	−	−	−	−	−	−	+	−
Age wheelchair-bound, y	13	16	17	9	9	9	9	8	8
Neuroimaging (MRI)									
Cerebellar atrophy	−	+	−	+	+	−	−	−	−
WM involvement (hypomyelination)	+	+	+	+	+	+	+	+	+
Thin CC	+	+	+	+	+	+	+	+	+
Hepatic involvement									
Age at onset, y	3	4	3	3	8	7	5	5	n.a.
Elevated liver enzymes (age)	+(3)	+(4)	+(3)	+(3)	+(8)	+(8)	+(5)	+(5)	n.a.
Liver biopsy	−	−	−	+(HF)	+(HF)	−	−	+(HF)	−
Abnormal ultrasonography	+	+	+	+	+	+	+	+	−
Heart involvement									
Dilated cardiomyopathy (age at onset, y)	+(18)	+(17)	+(15)	+(9)	+(10)	+(9)	+(9)	+(8)	+(10)
Deafness									
Sensorineural hearing loss (age at onset, y)	+(7)	+(9)	+(9)	+(9)	+(6)	+(8)	+(5)	+(7,5)	+(7)

CC = corpus callosum; DD = developmental delay; dx = diagnosis; F = female; HF = hepatic fibrosis; ID = intellectual disability; M = male; mo = months; na = not available; ofc = occipital cranial circumference; w = weeks; WM = white matter; y = years. [a]Southern Italy; [b]all homozygous; [c]birth parameters: birth weight (length/weight/OFC, in centiles); [d]At term; [e]Premature (33 weeks gestation); [f]At term; [g]At 36 weeks; [h]growth parameters: age: height; weight; ofc (height/weight/ofc, in centiles); [i]length.
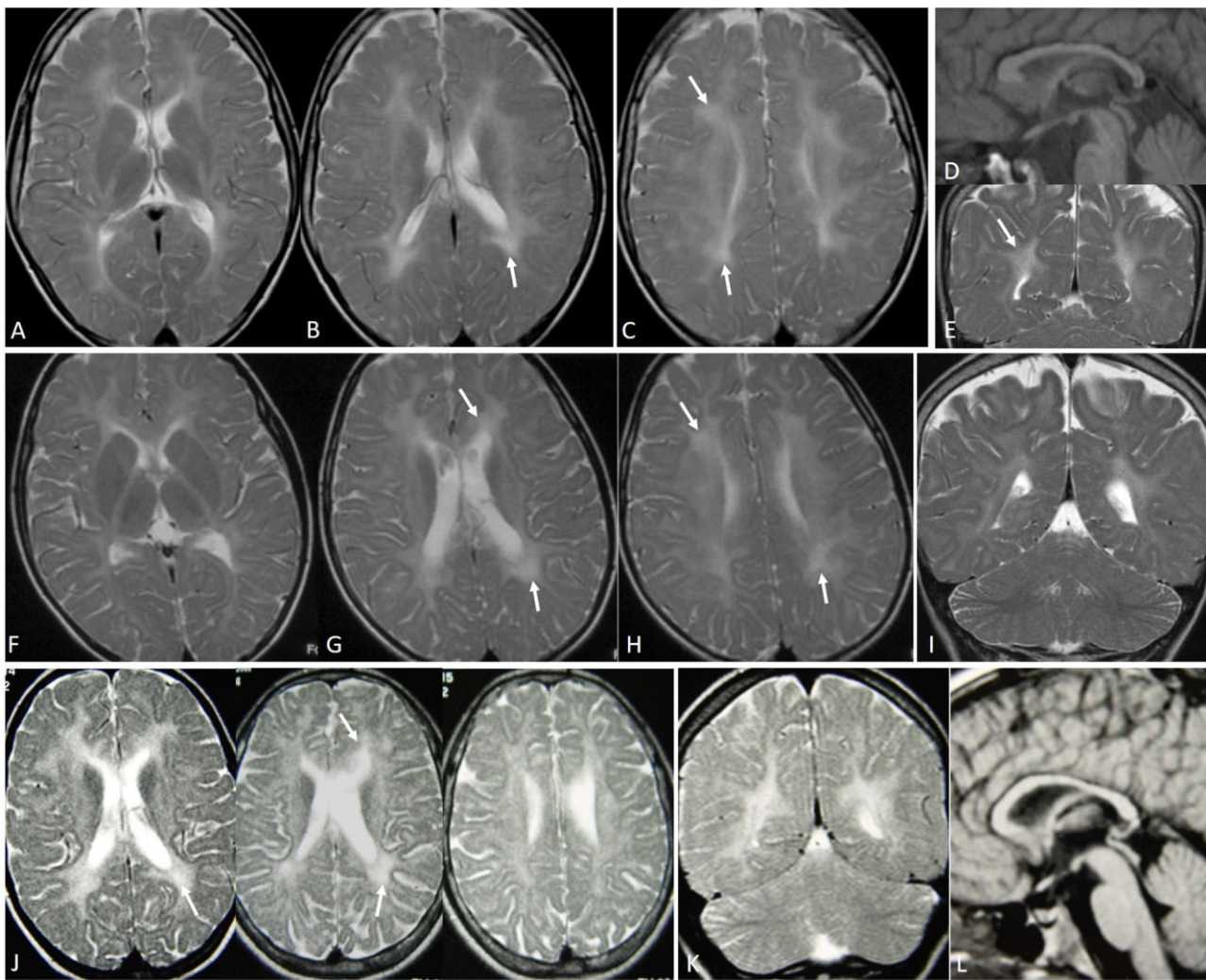
Figure 2 MRI characteristics of AR-LAD. (**A–E** and **I**) Pedigree 4, Patientt II, 1 at age 7 years; (**F–H**) Pedigree 3, Pt I, 3 at age 7 years; (**J–L**) Pedigree 1, Patient 3 at age 7 years. Images demonstrate similar findings: T_2-weighted images in **A–C** and **E–K** show diffuse T_2 hyperintensity in the white matter of the brain, suggesting a hypomyelinating leukoencephalopathy. T_2 hyperintense areas were particularly enhanced at the level of the periventricular white matter areas (arrows). Note the normal myelination of cerebellar white matter in **I** and **K** and the global corpus callosum thinning on T_1 weighted images (**D** and **L**).

portal fibrotic septa with chronic inflammation and parenchymal congestion and atrophy (Supplementary Fig. 2C).

More interestingly, histopathological analysis of the brain samples from an autopsy performed on Patient 3 in Pedigree 1[18] showed microvacuolar changes of the neuropil (Supplementary Fig. 3A and B), with no effects on astrocyte proliferation or axonal spheroids (Supplementary Fig. 3A and B). Moreover, Luxol fast blue staining, to label myelin in the white matter, showed severe hypomyelination and diffuse gliosis, when compared with the control (Supplementary Fig. 3E and F).

RNF220 tissue expression profile and its localization in the CNS

We assessed the *RNF220* tissue expression profile using a commercial cDNA panel from different human adult tissues (Supplementary Fig. 4A). In accordance with the expression data deposited in public databases (GTEX, BioGPS and SAGE), RT-qPCR analysis revealed the ubiquitous expression of *RNF220*, which is abundant in brain and spinal cord, particularly in the cerebellum and cerebral cortex (Supplementary Fig. 4A). We also determined *RNF220* mRNA levels in human foetal CNS, observing a higher

expression in the cerebellum, spinal cord and cortex (Supplementary Fig. 4B). Furthermore, we investigated the distribution of RNF220 protein in mouse CNS at age 8 days. To this aim, we conducted immunofluorescence studies on the hippocampus, cerebellum and telencephalon of mouse brain by using a polyclonal antibody against RNF220 in combination with neural and glial cell markers (GFAP, nestin, Smi32 and calbindin). A basal expression of RNF220 was observed in the hippocampus and telencephalon, while a prominent localization was appreciated in the cerebellum. In the dentate gyrus of the hippocampus, RNF220 was poorly detected, while it was predominantly observed in the molecular layer of CA1, CA2 and CA3 regions (Fig. 3). In the telencephalon and cerebellum, RNF220 staining was detected in mature neurons that express the neuronal marker Smi32 (Fig. 3). Conversely, no immunoreactivity of RNF220 was detected in astroglial cells that are immune-reactive for GFAP, or in neural progenitor cells, which are identified by the expression of nestin (Fig. 3). In particular, RNF220 was widely expressed in the cerebellum, where it was detected in the external granular layer, in deep cerebellar nuclei and in Purkinje cells, the latter specifically labelled by the anti-calbindin antibody (Fig. 3). Furthermore, while RNF220 in the hippocampus and telencephalon showed a predominantly
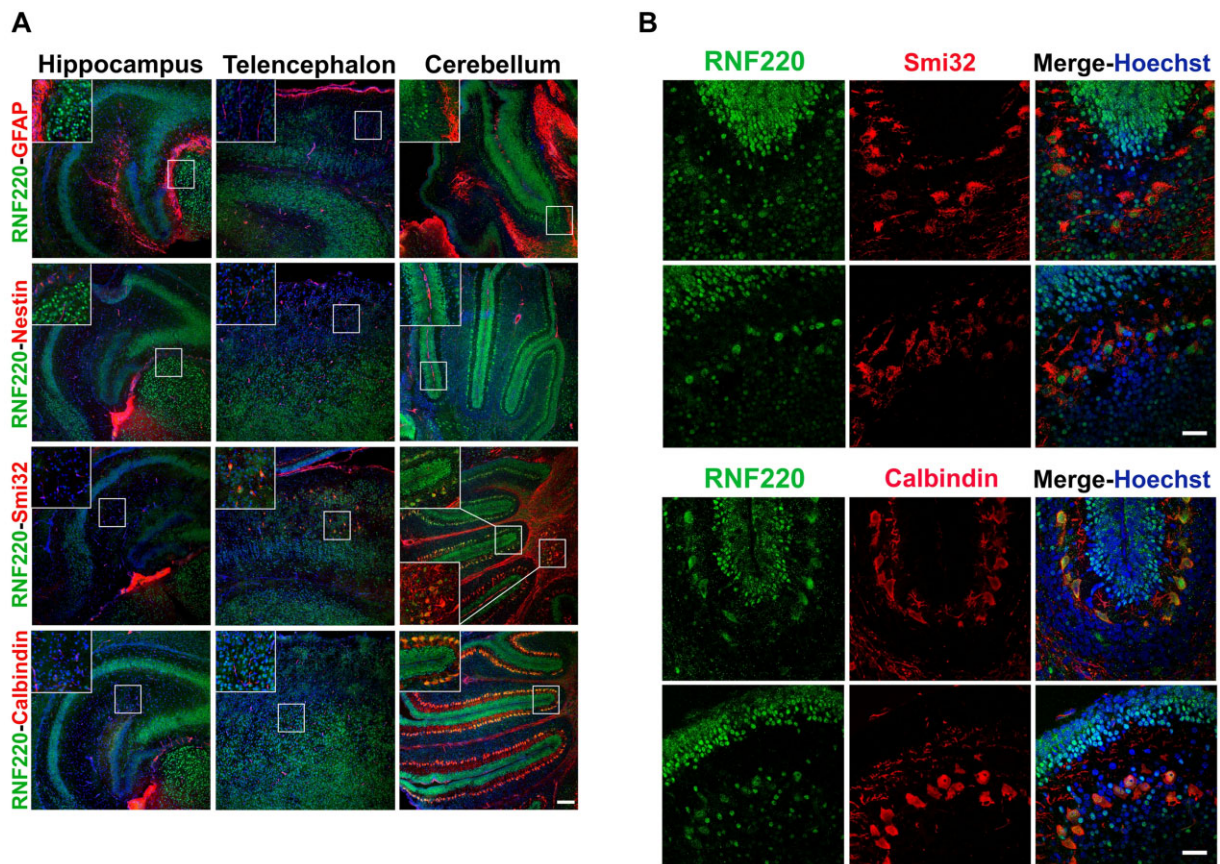
Figure 3 RNF220 immunohistochemical detection in the CNS of an 8-day-old mouse. (**A**) Significant expression of RNF220 is observed in the molecular layer of the hippocampus, in the telencephalon, with a conspicuous signal in the cerebellum. (**B**) *Top*: Sagittal brain sections from an 8-day-old mouse were stained for RNF220 in combination with the neural markers Smi32 and calbindin and the astroglial marker GFAP. Nuclei were counterstained with Hoechst (Scale bar = 100 μm). *Insets* are magnifications of the selected areas; Scale bar = 25 μm. *Bottom*: Higher magnification of sagittal cerebellum sections from 8-day-old mouse labelled for RNF220 in combination with the neuronal markers Smi32 and calbindin. Nuclei were counterstained with Hoechst. Scale bar = 25 μm.

cytoplasmic and perinuclear localization, it localized primarily to the nucleus in the cerebellar neurons (Fig. 3).

To characterize the expression pattern of RNF220 in neuronal cells, we investigated its localization at different stages of the *in vitro* differentiation of human iPSCs into motor neurons. As shown in Supplementary Fig. 5, at Day 0, RNF220 staining was weak and had a widespread cytosolic distribution, while at Day 5, when the first neurons appeared, RNF220 staining greatly increased and localized into the nucleus, according to the subcellular localization reported in the Human Protein Atlas. RNF220 localization remained clearly nuclear from Days 10 to 25 of *in vitro* differentiation. However, at Day 30, when differentiation was complete and motor neurons were mature, showing clearly defined axons and dendrites, RNF220 was widely distributed among the nucleus and neurites (Supplementary Fig. 5).

Subcellular localization of RNF220 protein in cell lines

To characterize the subcellular localization of wild-type and mutant RNF220, we subcloned the *RNF220* cDNA in different expression vectors. First, we demonstrated that the subcellular distribution of RNF220 was not affected by tag positioning (Supplementary Fig. 6A). Thus, we observed in COS-1 cells transiently transfected with pFLAG-CMV-6a vector encoding N-terminal FLAG-tagged RNF220 (wild-type and mutants) that RNF220 localized primarily to the nucleus (Supplementary Fig. 6A), which is

consistent with previous findings in HEK-293T transfected cells.[6] In the nucleus, RNF220 labels vesicle-like structures with a distribution that strongly recalls nuclear speckles, dynamic interchromatin clusters enriched in splicing factors, which continuously exchange factors with the nucleoplasm and transcriptionally active regions.[19] Recent reports describe that proteasomal-mediated protein degradation in the nucleus occurs in distinct nucleoplasmic foci, which partially overlap with nuclear speckles,[20] promyelocytic leukemia bodies[21] and clustosomes.[22] To assess whether the RNF220 vesicle-like structures co-localized with nuclear speckles, cells ectopically expressing wild-type RNF220 were labelled, in co-immunofluorescence experiments, with the antibody against ASF/SF2, a splicing factor enriched in nuclear speckles (Supplementary Fig. 6B). As shown, RNF220 significantly co-localized with ASF2/SF2, suggesting that RNF220 is enriched in nuclear speckles (Supplementary Fig. 6B). Furthermore, we explored the relationship between RNF220 and the ubiquitin proteasome system in COS-1 cells, by analysing, through immunofluorescence experiments, RNF220 co-localization with the 20S protein complex, the catalytic core of the 26S proteasome. The spatial relationship between RNF220 and 20S proteasome, examined by co-localization analysis of their confocal images, detected a partial co-distribution degree, thus suggesting a moderate link between the two molecules (Supplementary Fig. 6C).

Whilst wild-type RNF220 rarely forms vesicle-like structures in the cytoplasm, we observed that RNF220 mutant proteins (both

RNF220_R363Q and RNF220_R365Q) localized not only in nuclear speckles but also coalesced in the cytoplasm to form protein aggregates/inclusions (Fig. 4). This was confirmed by localizing RNF220 by immunofluorescence in a patient's primary fibroblasts, showing increased signal, with an abnormal increase in the cytoplasm, with increased immunofluorescence for the 20S proteasome (Fig. 5).

Proteomic identification of RNF220 interacting proteins

To gain insight into the cellular functions of RNF220, a proteomic analysis was performed to identify RNF220 interactors. The total lysates obtained from HEK-293T cells, either non-transfected (mock fraction) or expressing FLAG-tagged wild-type RNF220, were immunoprecipitated using anti-FLAG monoclonal antibody covalently linked to sepharose beads to isolate RNF220 and its binding partners. Proteins retained by RNF220 were separated by SDS-PAGE, purified and identified by LC-MS. Proteins retained by RNF220, but absent in the mock fraction, are listed in Supplementary Table 2. Considering the nuclear localization of RNF220, we focused our attention on the nuclear candidate proteins (Supplementary Fig. 7). Among the putative nuclear interactors, an enrichment of all members of the lamin protein family (i.e. lamin B1, lamin AC and lamin B2) was observed, suggesting a potential role of RNF220 in the functional regulation of lamin proteins.

RNAi-mediated downregulation of *Drosophila* RNF220 specifically affects the lamin B1 and causes neurodegeneration

To address the potential role of RNF220 in lamin protein regulation, we evaluated the effect of *RNF220* silencing on fly orthologues of the lamin protein family by downregulating *RNF220* expression in *Drosophila* tissues using the UAS-GAL4 system. First, we verified by RT-qPCR that the expression of a specific *RNF220* RNAi construct in larval muscles under control of Mef2-GAL4 driver at 18°C downregulated *RNF220* expression (Fig. 5A). Interestingly, the same RNAi construct causes adult fly lethality when expressed in larval muscles at 25°C. Furthermore, we observed that RNAi-mediated downregulation of *RNF220* late during eye development, under GMR-GAL4 at 25°C, caused a striking neurodegeneration of the retina (Fig. 5B, top). Moreover, repression of *RNF220* early during fly eye and salivary gland development at 25°C, under control of eyeless-GAL4, causes adult fly lethality. Moreover, the same flies grown at the lower temperature of 18°C, which reduced RNAi expression, showed severe alterations in eye development linked to a significant reduction in the eye surface (Fig. 5B, bottom). Finally, to assess the effects of *RNF220* downregulation on the localization of fly orthologues of the lamin protein family, we prepared salivary gland cells from fly larvae expressing *RNF220* RNAi under eyeless-GAL4 at 25°C. Although these conditions cause adult lethality, they are compatible with larval development. *RNF220* repression in fly salivary gland cells significantly and specifically altered the subcellular localization of lamin Dm0, the fly orthologue of human lamin B1, and promoted its accumulation (Fig. 5C). Interestingly, no effect was observed on the subcellular localization and expression levels of the fly orthologue of lamin A/C (lamin C) in the same preparation (Fig. 5D).

AR-LAD mutations affect RNF220 binding activity for lamin B1

Based on the interactome data and the specific impact of *RNF220* silencing on the localization and accumulation of the fly orthologue of lamin B1, we investigated the association of endogenous RNF220 and lamin B1 using subcellular fractionation and co-immunoprecipitation experiments. Firstly, we compared the distribution of RNF-220 and lamin B1 in subcellular fractions of nuclei from mouse cerebellum (Supplementary Fig. 9A), which showed high expression of RNF220 (Fig. 3). Interestingly, RNF220 and lamin B1 showed a similar distribution with substantial enrichment in the nuclear matrix fraction, which contained a very low amount of total proteins (Supplementary Fig. 9A). Thus, we immunoprecipitated lamin B1 from solubilized proteins extracted from the nuclear matrix of cerebellar cells, and we demonstrated a significant interaction of endogenous lamin B1 with RNF220 (Fig. 6A). Furthermore, to assess how the mutations affect RNF220 binding activity to lamin B1, we performed co-immunoprecipitation experiments on nuclear lysates from HEK-293T cells transfected with RNF220 constructs. Thus, we observed that both RNF220 mutants showed reduced binding to endogenous lamin B1 compared with the wild-type (Fig. 6B). Reduction was particularly evident if we normalized the amount of retained lamin B1 for the corresponding level of each immunoprecipitated RNF220 variant (Fig. 6B). Interestingly, p.R365Q substitution affected lamin B1 binding more seriously compared with the p.R363Q mutation (Fig. 6B).

To gain insights on the molecular mechanisms underlying the role of RNF220 in the regulation of lamin B1, we assessed the effects of RNF220 expression on lamin B1 stability and ubiquitination in nuclear extracts. Since it has already been established that lamin B1 can be degraded through ubiquitin-proteasome pathways[23] as well as via autophagy,[24] we co-expressed RNF220 and lamin B1 with tagged ubiquitin with and without bafilomycin, a lysosomal inhibitor which specifically blocks the autophagy flux (Supplementary Fig. 9B). Thus, although lamin B1 was ubiquitinated in the absence of RNF220, its ubiquitination increased in the presence of the wild-type RNF220, and more intriguingly, RNF220 mutants significantly reduced the ubiquitination of nuclear lamin B1 (Supplementary Fig. 9B). Noticeably, such effects were evidenced by the treatment with bafilomycin, suggesting a role for RNF220 in the processes of ubiquitination and autophagy (Supplementary Fig. 9B).

The nuclear lamina morphology of fibroblasts is affected by p.R363Q and p.R365Q mutations

Considering the nuclear localization of RNF220, its binding to lamin B1, one of the major components of the nuclear lamina, and the effects of *RNF220* downregulation in *Drosophila*, we assessed the effects of *RNF220* mutations on the morphology of nuclear envelop in AR-LAD skin fibroblasts. Firstly, we verified fibroblasts as valuable system to model AR-LAD, by evaluating the expression level of *RNF220* in these cells. Evidence from the EST database suggests the presence of at least six alternatively splice variants of *RNF220* mRNA: three that encode full-length protein RNF220-202/203/204 (ENST00000355387, ENST00000361799, ENST00000372247); and three additional splice variants RNF220-201 (ENST00000335497), RNF220-205 (ENST00000440132) and RNF220-206 (ENST00000453863), that encode for shorter isoforms. Specific primer pairs able to detect all transcripts were exploited in RT-qPCR experiments from AR-LAD and control skin fibroblasts (Supplementary Fig. 8A). As shown in Supplementary Fig. 8B, RT-qPCR analysis showed the expression of different *RNF220* variants in primary fibroblast culture. Specifically, while variants 201, 205 and 206 were amplified in fibroblasts, the full-length variants were not detected in these cells, according to their brain specific expression (Supplementary Fig. 8B). Furthermore, we assessed the expression of the different spliced variants in fibroblasts of healthy and AR-LAD affected individuals, and we confirmed that variants 201, 205 and 206 are expressed in all genetic backgrounds. Thus,
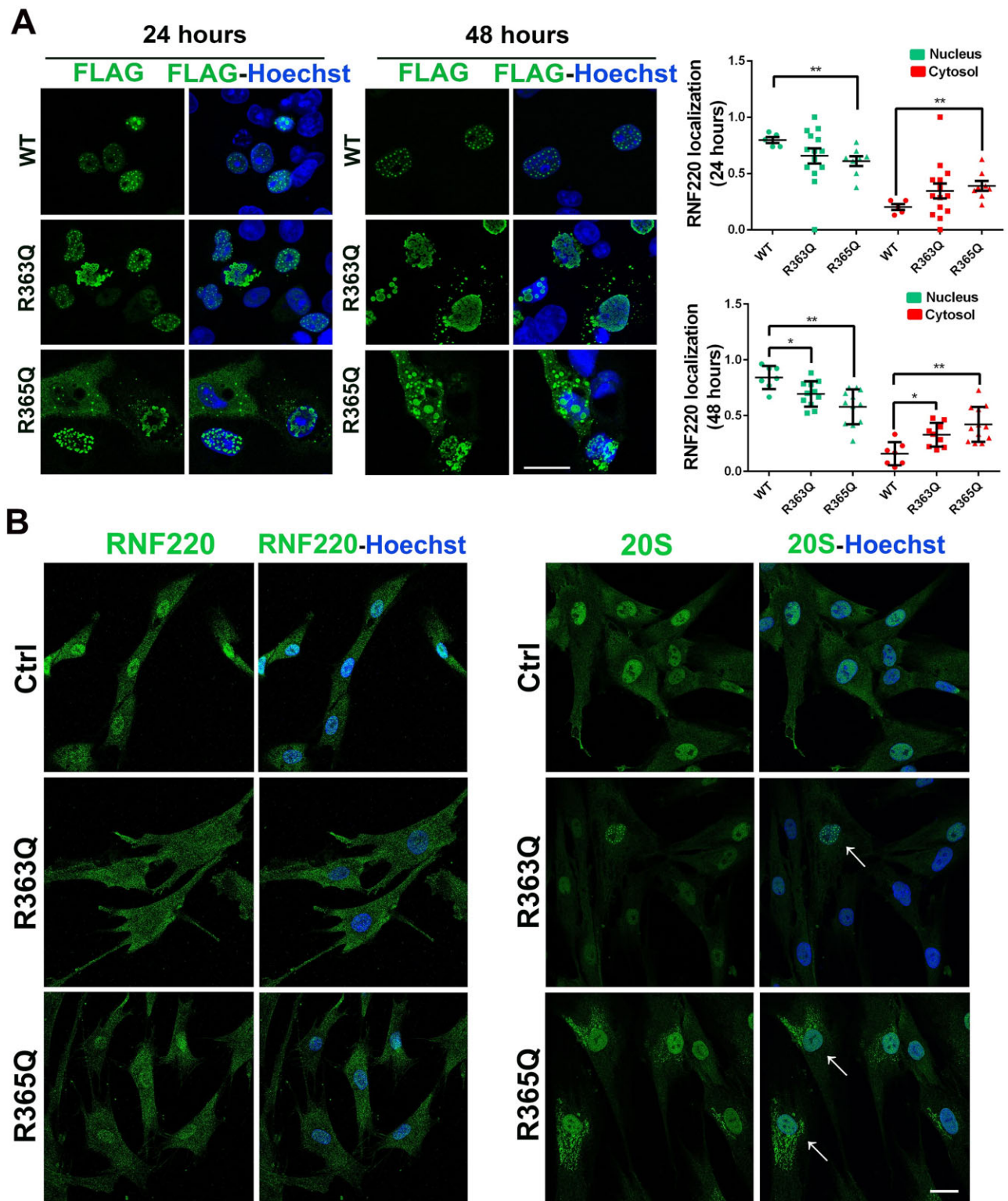
Figure 4 RNF220 subcellular localization in COS-1 cells at different times of transfection and RNF220 and 20S-proteasome subcellular localizations in AR-LAD primary fibroblasts. (A, *left*) COS-1 cells transfected using 1 μg of FLAG-tagged RNF220 (wild-type or mutants) were immunostained with the anti-FLAG antibody and Hoechst, after 24 h of transfection. Scale bar = 25 μm. Bar graph indicates the frequency of nuclear and cytosolic localization of RNF220 (wild-type and mutants). Results are presented as mean ± SEM (*n* = 123 cells from wild-type, 141 cells from R363Q and 135 cells from R365Q). Student's *t*-test, **P ⩽ 0.01. *Right*: COS-1 cells expressing FLAG-tagged RNF220 (wild-type or mutants) were immunostained with the anti-FLAG antibody and Hoechst after 48 h of transfection. Scale bar = 25 μm. Results are presented as mean ± SEM (*n* = 150 cells from wild-type, 123 cells from R363Q and 137 cells from R365Q). Student's *t*-test, *P ⩽ 0.05, **P ⩽ 0.01. (**B**, *left*) Primary fibroblasts obtained from healthy (control) and AR-LAD patients were immunostained with the anti RNF220 antibody and Hoechst. Scale bar = 25 μm. AR-LAD fibroblasts showed a preferential cytosolic localization of RNF220, compared with the control fibroblasts. *Right*: Primary fibroblasts obtained from healthy and AR-LAD patients were immunostained with the anti 20S-proteasome antibody and Hoechst. Scale bar = 25 μm. In the control fibroblasts, the 20S-proteasome presents a nuclear diffuse distribution. In the AR-LAD fibroblasts harbouring the p.R365Q substitution, the 20S-proteasome forms a cytosolic aggregate, suggesting flooding of the overall proteolytic capacity. In AR-LAD cells harbouring the p.R363Q mutation, nuclear aggregates of the 20S-proteasome are observed.
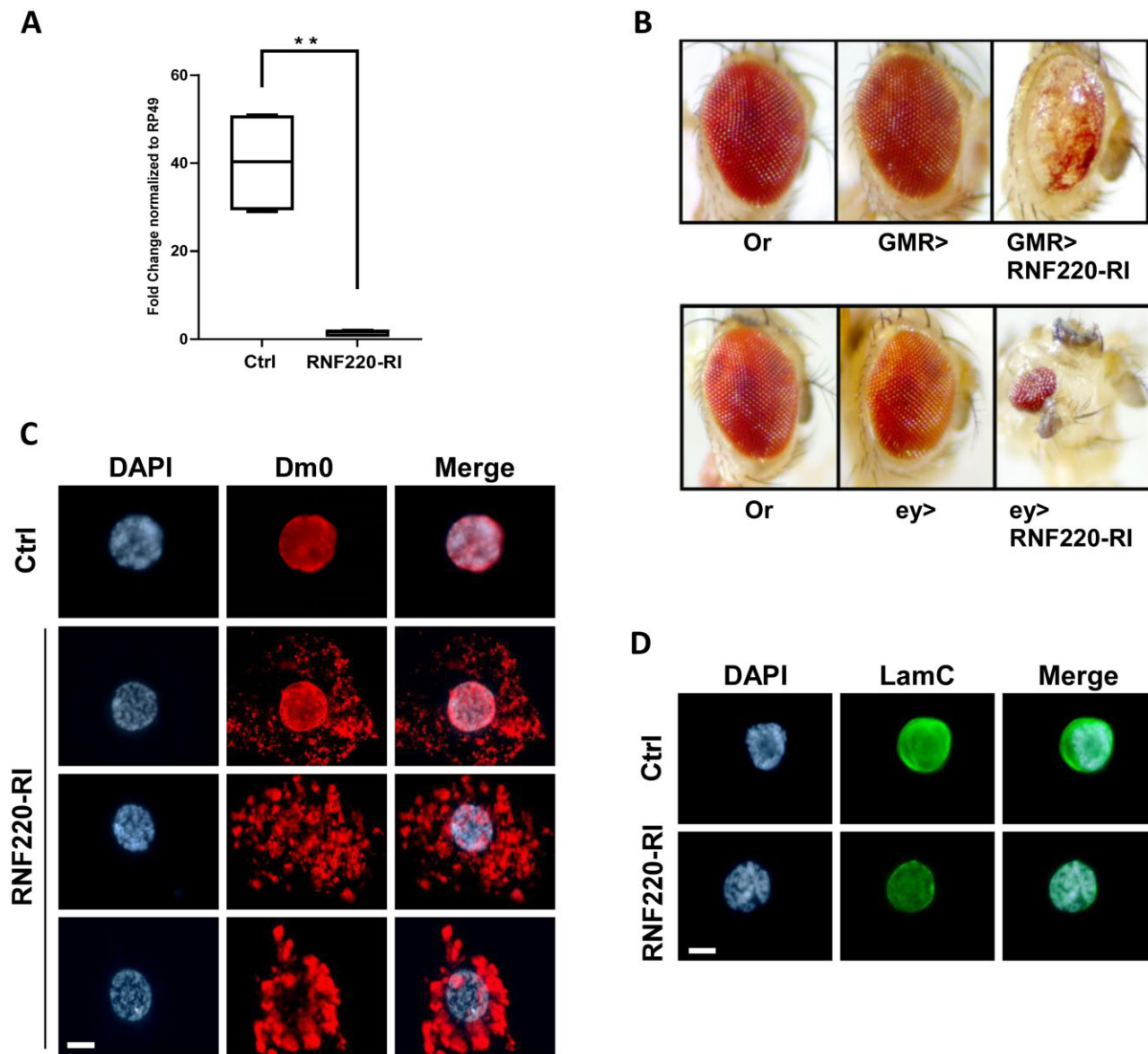
Figure 5 Effects of RNAi-mediated downregulation of the RNF220 *Drosophila* orthologue in different fly tissues. (**A**) Expression in fly muscle of a specific RNAi construct that targets fly RNF220, under control of the Mef2-GAL4 driver, at 25°C, caused adult fly lethality. Total RNA extracted from fly larvae expressing UAS-RNF220-RNAi under Mef2-GAL4, or the driver alone, was analysed by RT-qPCR. Relative levels of RNF220 transcript between genotypes are shown. The SEM was calculated from *n* = 3 independent experiments. *$P < 0.05$. (**B**) RNAi-mediated downregulation of RNF220 significantly affects fly eye development. Flies expressing RNF220 RNAi construct late during eye development, under GMR-GAL4, show strong retina degeneration at 25°C (*top*). Expression of the same RNAi construct early during eye development, under eyeless-GAL4, causes fly lethality at 25°C. Flies grown at 18°C show severe alterations of eye morphology and a significant reduction of eye surface (*bottom*). (**C**) RNAi repression of RNF220 in larval salivary glands strongly affects the subcellular localization of lamin Dm0 and promotes its accumulation. Salivary gland cells were dissected from fly larvae expressing UAS-RNF220-RNAi under eyeless-GAL4, or eyeless-GAL4 on its own, and stained in immunofluorescence experiments with antibodies against lamin Dm0. Different rates of lamin Dm0 accumulation and the different kinds of protein aggregate are shown. (**D**) Immunofluorescence labelling with antibodies against lamin C of cells from the same genotypes was used as a control. Scale bars = 10 μm.

although the *RNF220* full-length variant is not expressed, other isoforms containing the protein domains carrying AR-LAD mutations are expressed in fibroblasts.

Confocal analysis of AR-LAD fibroblasts, immunostained with different nuclear envelope markers, shows abnormal nuclear shapes in patient cells, significantly more frequent than controls, with multiple invaginations and lobulations (Fig. 7).

Discussion

Here, we describe a rare form of hypomyelinating leukodystrophy manifesting as progressive ataxia, mild intellectual disability and deafness. As the disease progresses, patients experience sensoryneural deafness, resulting in complete hearing loss by their first decade of life. Moreover, during the follow-up most patients show signs of hepatopathy with increased AST (aspartate aminotransferase) and ALT (alanine aminotransferase), which is associated with periportal fibrosis at liver biopsy. Most importantly, all patients during the late follow-up develop a fatal cardiomyopathy
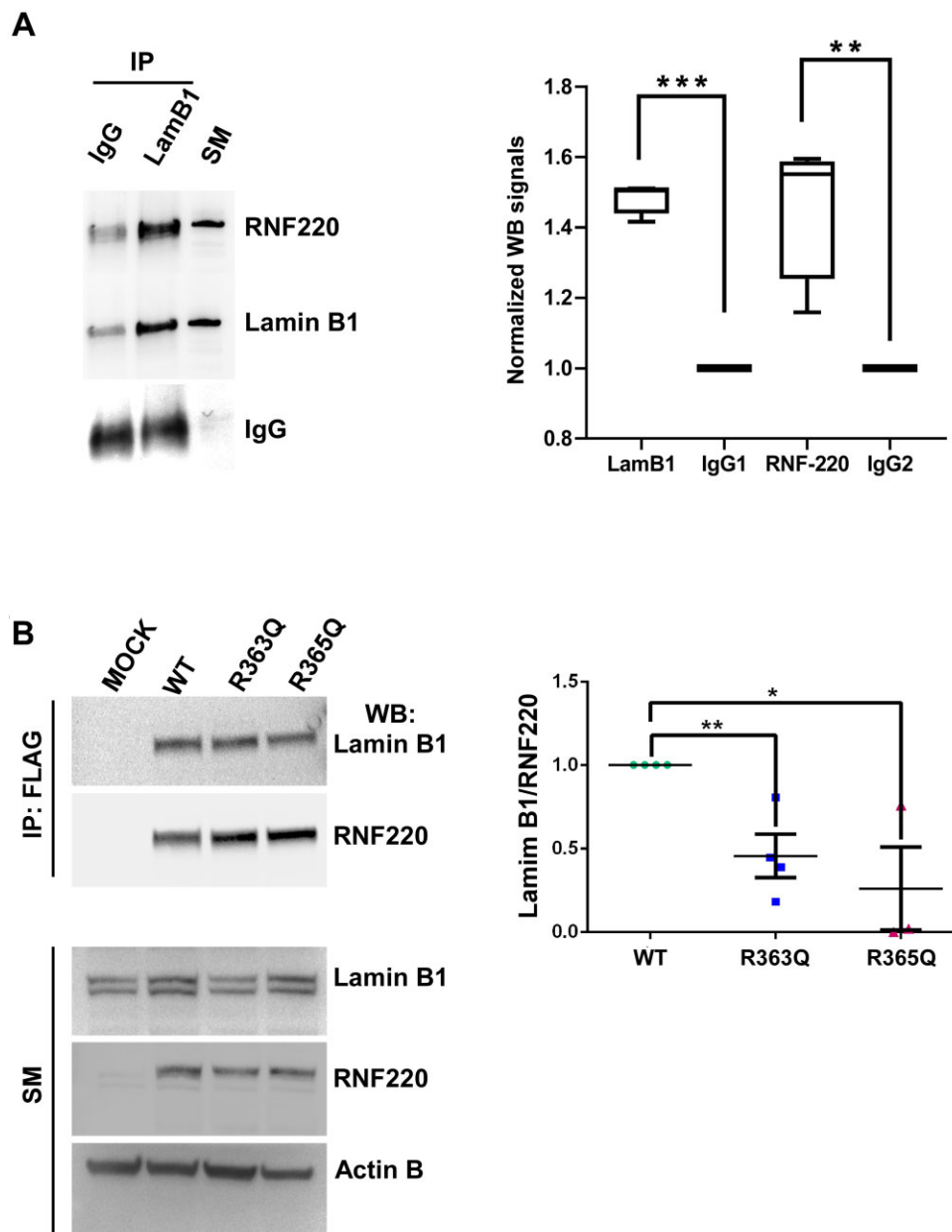
Figure 6 Co-immunoprecipitation of lamin B1 and RNF220 from cerebellum extract showing tight link between RNF220 and lamin B1. (**A**) Proteins in RIPA buffer were immunoprecipitated with anti-lamin B1 antibody or mouse IgG, as a negative control. Proteins retained on the beads were separated by SDS-PAGE and analysed by western blotting with corresponding antibodies. A 1:50 dilution of extract was utilized for each immunoprecipitation as the starting material (SM), and a 1:2 dilution of bound proteins was used as the immunoprecipitated material (IP). Western blotting signals from two independent experiments, normalized on the amount of IgG, were acquired by Fiji NIH ImageJ software, and their statistical significance was assessed using GraphPad Prism software (version 8.0) with one-way ANOVA analysis according to Sidak's multiple comparisons test. $**P < 0.01$, $***P < 0.001$ (*left*). (**B**) RNF220 interacts with proteins of the nuclear lamina. The effect of p.R363Q and p.R365Q substitution on RNF220 binding activity for lamin B1. The nuclear fraction of HEK-293T cells expressing FLAG-tagged RNF220 (wild-type or mutants) were subjected to immunoprecipitation experiments using the anti-FLAG monoclonal antibody covalently attached to sepharose beads to detect the interaction between RNF220 and endogenous lamin B1. Both R363Q and R365Q substitutions showed reduced binding to lamin B1 compared with wild-type RNF220 when the amount of lamin B1-bound was normalized for the level of RNF220 pulled down. The graph shows the densitometric quantification of lamin B1 retained by each RNF220 protein variant. Results are presented as mean ± SEM. $n = 3$, Student's t-test,$*P \leqslant 0.05$.

that leads to death by the end of the second decade. Following the peculiar clinical and neuroradiological characteristics, we define this new type of white matter disease as a novel form of leukodystrophy with autosomal recessive pattern of inheritance and associated with ataxia and deafness. The MRI in patients affected by AR-LAD corresponds to a hypomyelinating leukodystrophy that diffusely involves the entire white matter including the subcortical U-fibres and the internal capsule, with abnormal T_2 hyperintensity

that is particularly enhanced at the level of the periventricular areas (Fig. 3). Moreover, hypomyelination characteristically spares the cerebellar and the brainstem white matter (Fig. 3). The distribution of hypomyelination differs from that described in ADLD related to *LMNB1* duplication, where T_2 symmetric diffuse hyperintensities generally spare U-fibres as well as the periventricular white matter in the brain and involve the upper and middle cerebellar peduncles.[25]
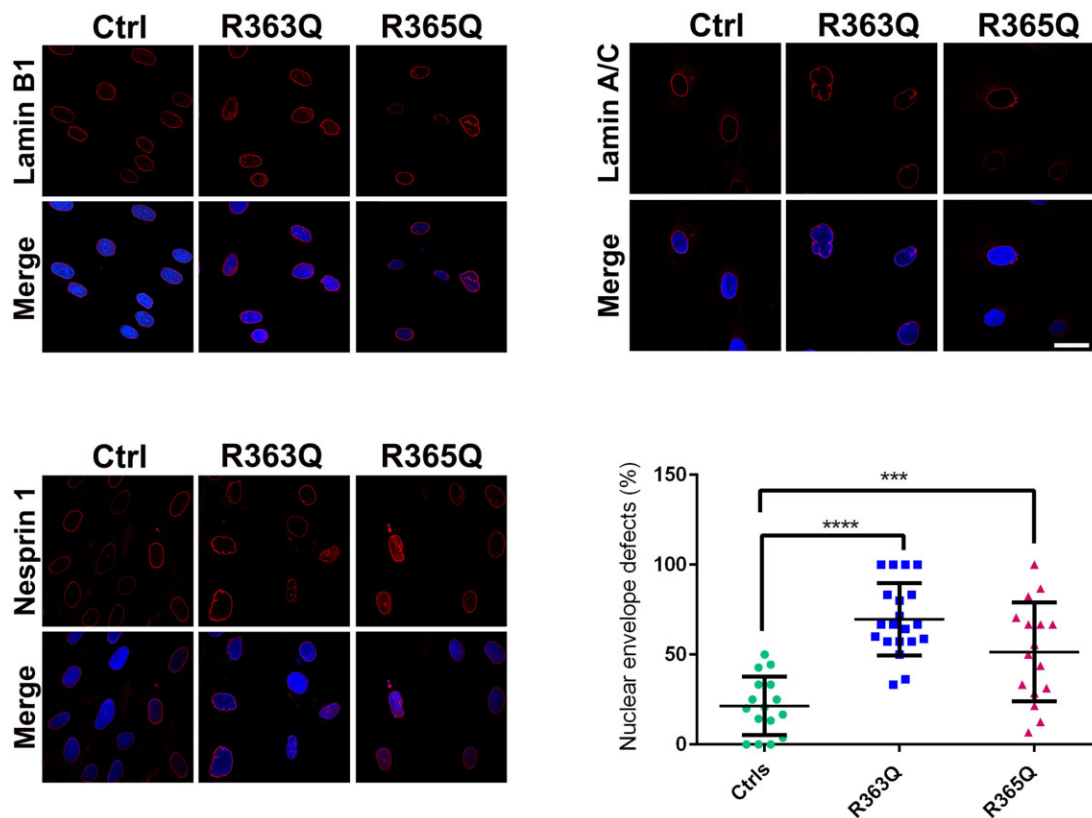
Figure 7 RNF220 mutations affect nuclear envelop integrity by altering lamin and nesprin localization in AR-LAD fibroblasts. Primary fibroblasts of healthy (Ctrl) and AR-LAD-affected (R363Q and R365Q) individuals were labelled with lamin B1, lamin A/C and nesprin 1 antibodies and counterstained with Hoechst. Scale bar = 25 μm. The nuclear envelope of the AR-LAD fibroblasts shows abnormal invaginations and lobulations and increased levels of all markers (lamin B1 A/C and nesprin1). The bar graph indicates the frequency of cells with nuclear envelope defects and irregular nuclear margins. Results are presented as the mean ± SEM (*n* = 251 cells from the wild-type, 177 from R363Q and 186 cells from R365Q). Student's *t*-test, ****$P \leqslant 0.001$, ***$P \leqslant 0.005$.

Whole exome sequencing analysis allowed us to identify *RNF220* as the causative gene for AR-LAD, and two different homozygous mutations in two highly conserved and close residues (Fig. 1B) in exon 8, c.1088G > A (p.R363Q) and c.1094G > A (p.R365Q), were identified in patients with AR-LAD. In the Roma families, we demonstrated a founder effect of the p.R365Q mutation, for which we did not find any homozygosity in the major control general population database (gnomAD), although genomic databases limited to Roma populations are not yet available. The phenotype-genotype correlation shows that individuals carrying the biallelic p.R365Q mutation are more severely affected and die around the end of the first decade, only few years after the onset of cardiomyopathy, while subjects harbouring the homozygous p.R363Q mutation survive until the end of the second decade, according to the later onset of cardiomyopathy. Although we have not completely elucidated the reasons for this difference, it is interesting to note that the loss of binding activity of p.R365Q mutants to lamin B1 and its propensity to form cytoplasmic aggregations are more exacerbated than the p.R363Q mutant. Intriguingly, these mutations show comparatively different activity on lamin B1 in the *in vitro* ubiquitination assay (Supplementary Fig. 9B).

RNF220 has previously been described as a RING finger protein with E3 ubiquitin ligase activity,[4] which is highly expressed in the developing mouse nervous system[5,6] and is involved through modulating Sonic hedgehog/GLI signalling in ventral spinal cord patterning[5,6] and cerebellum development.[8] E3 ubiquitin ligases are key components of the ubiquitin-proteasome system, one of the major cellular routes for eliminating misfolded proteins,[26,27] and

catalyse the covalent attachment of one or more ubiquitin moiety to their target proteins. These modifications exert diverse effects, ranging from proteasome-dependent proteolysis to post translational modifications that modulate protein function, structural conformation and subcellular localization.[28–31]

Consistent with previous studies,[5,6,8] we observed the widespread expression of RNF220 in the mouse CNS, with a predominant localization in the cerebellum: in the external granular layer, deep cerebellar nuclei and Purkinje cells (Fig. 4). Moreover, according to its reported role in the mouse spinal cord and cerebellum pattern formation,[5,6,8] we detected high expression levels of human *RNF220* mRNA in foetal and adult spinal cord as well as cerebellum (Supplementary Fig. 4).

To characterize the effect of AR-LAD-linked mutations on the subcellular localization of RNF220, we expressed wild-type and mutant RNF220 variants in COS-1 cells and observed their preferential nuclear localization (Supplementary Fig. 6A). We showed that wild-type RNF220 protein mainly localizes in the nuclear speckles as demonstrated by the co-localization with ASF/SF2 (Supplementary Fig. 6B). Interestingly, nuclear speckles, apart from their well-known role in interchromatin clusters enriched in premRNA splicing factors, are likely to be involved in protein degradation via the ubiquitin-proteasome system.[20] Accordingly, we observed the co-localization of RNF220-positive nuclear speckles with the 20S proteasome complex, although this was not highly significant (Supplementary Fig. 6C). RNF220 carrying p.R363Q and p.R365Q mutations do not localize exclusively in nuclear speckles, but also coalesce into the cytoplasm to form protein inclusions.

This observation strongly suggests that AR-LAD mutations affect the subcellular localization of RNF220 and increase its cytoplasmic aggregation (Fig. 5).

We used a proteomic-based approach to identify RNF220 binding partners. Mass spectrometry analysis detected, among the RNF220 nuclear binding proteins, all components of the lamin protein family: lamin B1, lamin AC and lamin B2 (Supplementary Fig. 7). By RNAi-mediated downregulation of *RNF220* in different fly tissues, we demonstrated that *RNF220* silencing affects the subcellular localization of lamin Dm0, the fly orthologue of lamin B1, promoting its aggregation and neurodegeneration (Fig. 5). Furthermore, *RNF220* silencing does not affect the subcellular localization of the fly orthologue of lamin A/C, suggesting that *RNF220* dysregulation primarily targets lamin B1. Thus, we validated, by co-immunoprecipitation experiments, RNF220 and lamin B1 protein association and demonstrated that AR-LAD mutations, particularly p.R365Q, significantly diminish RNF220 binding to lamin B1.

Lamin B1, encoded by the *LMNB1* gene, is a member of the intermediate filament protein family and is part of the nuclear lamina, the protein meshwork lining the inner surface of the nuclear envelope.[32,33] Nuclear lamina not only provide mechanical support to the nucleus, but also play a dynamic role in the organization and regulation of chromatin, transcription, DNA replication, DNA repair and epigenetic modifications.[34–40] Lamin B1 is critical to proper brain development[41–45] and the entire CNS is susceptible to modifications in *LMNB1* levels.[11,12,46–48] The duplication of *LMNB1* or a large deletion of 660 kb upstream of this gene, which dysregulate the *LMNB1* gene dosage in brain tissue, have been reported to cause a severe progressive demyelinating disorder represented by an adult form of dominant leukodystrophy.[11,12,48–51] Patients with ADLD exhibit increased levels of lamin B1 transcript and protein in specific degenerating cerebral areas, indicating that abnormal levels of lamin B1 have deleterious consequences.[11,12] Interestingly, AR-LAD hypomyelination concurs with the deficiency in myelin deposition observed in ADLD and suggests that the reduced interaction of RNF220 with lamin B1 may selectively affect oligodendrocytes and neurons, which are the most sensitive cells to lamin B1 dysregulation.[11,52–58] Indeed, it has been observed that lamin B1 overexpression in oligodendrocytes leads to a premature differentiation arrest and suppression of myelin biosynthesis.[53] Accordingly, lamin B1 is tightly regulated during brain development, showing an expression pattern complementary to that of several myelin proteins,[55] and, in particular, oligodendrocyte differentiation is characterized by a progressive decline of lamin B1 expression.[59] Furthermore, lamin B1 levels vary during neurogenesis[60,61] and differentially regulate axon and dendrite outgrowth.[58] This tight modulation of the lamin B1 protein dosage implies the involvement of specific regulatory mechanisms. Recent studies have highlighted an important role of the ubiquitin-proteasome system in lamin B1 turnover,[62–64] and different E3 ligases, such as RNF123 and HECW2, have been reported to bind and target lamin B1 for proteasome proteolysis.[62,63] Moreover, the overexpression of human lamin B1 in *Drosophila* eyes causes a retina neurodegeneration[11] that strongly resembles the phenotype observed in flies expressing the *RNF220* RNAi construct (Fig. 5). According to the nuclear localization of RNF220, and its functional connection with lamin B1, we investigated the impact of RNF220 mutations on nuclear lamina morphology in AR-LAD primary fibroblasts. Morphological analysis of the nuclear envelope in AR-LAD fibroblasts revealed a higher frequency of blebs, herniations and honeycomb structures, which are typically observed in laminopathic patient cells (Fig. 7). These findings confirm the involvement of RNF220 in the maintenance of nuclear integrity and allow us to

hypothesize that the cardiomyopathy developed by patients may be related to a secondary laminopathy.

Indeed, the fatal dilated cardiomyopathy with diffuse fibrosis seen in AR-LAD is suggestive of the cardiomyopathy observed in patients affected by laminopathies.[65–67] Laminopathic patients harbour mutations in the *LMNA* gene, encoding A-type lamins (lamin A–C), two structural components of the nuclear lamina or in other genes encoding proteins functionally related to lamin A–C.[68]

Therefore, in light of these pieces of evidence we cannot exclude that RNF220 mutations may impair its binding to additional lamins, and that other laminar proteins may contribute to the morphological alterations observed in AR-LAD cells. Indeed, several indications link, directly or indirectly, laminopathies to an impairment of the ubiquitin-proteasome system.[69–71] Specific components of this system are activated by lamin misexpression,[69,72,73] and clearance of the inner nuclear membrane proteins has been reported to be proteasome-mediated.[74,75] Furthermore, some deleterious mutations of the lamin A–C proteins specifically affect their interaction with ubiquitin E3 ligases.[63,73,76] It has also been reported that components of nuclear lamina are degraded by the autophagy machinery through a direct interaction of lamin B1 with LC3, a major regulator of autophagy, in a specific transport from the nucleus to cytoplasm which ends with lysosomal degradation.[24]

Unfortunately, we had no direct access to any affected post-mitotic tissue of patients, such as the brain, which is the tissue mainly affected by AR-LAD leukodystrophy, to verify a possible accumulation of lamin proteins in degenerating cerebral areas. Although the absence of patient's autoptic tissues represent a great limitation, our *in vitro* and *in vivo* experiments strongly support the involvement of RNF220 in lamin B1 turnover and potentially that of other lamin proteins.

Finally, mutations in genes encoding proteins of the linker of nucleoskeleton and cytoskeleton (LINC) complex, which associates the nuclear lamina to the cytoskeleton, have been reported to cause hereditary hearing loss.[78,79] In mice deficient in the structural proteins of this complex fail to maintain the basal localization of their nuclei and degenerate as hearing matures.[77,78] Considering that all patients with AR-LAD experienced sensory-neural deafness resulting in complete hearing loss within the first decade, it is tempting to hypothesize that alterations of nuclear lamina in AR-LAD cells may impair its connection with the cytoskeleton via the LINC complex, causing hearing loss. Accordingly, it has also been recently observed in *Drosophila* that mutations in the Parkin-like E3 ubiquitin ligase Ariadne-1, which regulates the LINC complex, alter the nuclear morphology of larval muscles, and rare variants of the human homologue of this gene are associated with thoracic aortic aneurysms due to aberrant nuclear envelop function in smooth muscle cells.[79]

Overall, our findings shed new light on RNF220 nuclear functions and strongly suggest that RNF220 may play a key role in the maintenance of nuclear integrity by regulating laminar proteins.

Acknowledgements

Funding

Competing interests

The authors report no competing interests.

Supplementary material

Supplementary material is available at *Brain* online.

References

1. van der Knaap MS, Bugiani M. Leukodystrophies: A proposed classification system based on pathological changes and patho-genetic mechanisms. *Acta Neuropathol*. 2017;134(3):351–382.
2. Lin DS, Ho CS, Huang YW, et al. Impairment of proteasome and autophagy underlying the pathogenesis of leukodystrophy. *Cells*. 2020;9(5):1124.
3. Kohlschütter A, Eichler F. Childhood leukodystrophies: A clinical perspective. *Expert Rev Neurother*. 2011;11(10):1485–1496.
4. Kong Q, Zeng W, Wu J, Hu W, Li C, Mao B. RNF220, an E3 ubiquitin ligase that targets Sin3B for ubiquitination. *Biochem Biophys Res Commun*. 2010;393(4):708–713.
5. Kim J, Choi TI, Park S, Kim MH, Kim CH, Lee S. Rnf220 cooperates with Zc4h2 to specify spinal progenitor domains. *Development*. 2018;145(17):dev165340.
6. Ma P, Song NN, Li Y, et al. Fine-tuning of Shh/Gli signaling gradient by non-proteolytic ubiquitination during neural patterning. *Cell Rep*. 2019;28(2):541–553.e4.
7. Ma P, Song NN, Cheng X, et al. ZC4H2 stabilizes RNF220 to pattern ventral spinal cord through modulating Shh/Gli signaling. *J Mol Cell Biol*. 2020;12(5):337–344.
8. Ma P, An T, Zhu L, et al. RNF220 is required for cerebellum development and regulates medulloblastoma progression through epigenetic modulation of Shh signaling. *Development*. 2020; 147(21):dev188078.
9. Zhang L, Ye M, Zhu L, et al. Loss of ZC4H2 and RNF220 inhibits neural stem cell proliferation and promotes neuronal differentiation. *Cells*. 2020;9(7):1600.
10. Song NN, Ma P, Zhang Q, et al. Rnf220/Zc4h2-mediated monoubiquitylation of Phox2 is required for noradrenergic neuron development. *Development*. 2020;147(6):dev185199.
11. Padiath QS, Saigoh K, Schiffmann R, et al. Lamin B1 duplications cause autosomal dominant leukodystrophy. *Nat Genet*. 2006; 38(10):1114–1123.
12. Giorgio E, Robyr D, Spielmann M, et al. A large genomic deletion leads to enhancer adoption by the lamin B1 gene: A second path to autosomal dominant adult-onset demyelinating leukodystrophy (ADLD). *Hum Mol Genet*. 2015;24(11):3143–3154.
13. Compagnucci C, Piermarini E, Sferra A, et al. Cytoskeletal dynamics during in vitro neurogenesis of induced pluripotent stem cells (iPSCs). *Mol Cell Neurosci*. 2016;77:113–124.
14. Dignam JD, Lebovitz RM, Roeder RG. Accurate transcription initiation by RNA polymerase II in a soluble extract from isolated mammalian nuclei. *Nucleic Acids Res*. 1983;11(5):1475–1489.
15. Randles KN, Lam Le T, Sewry CA, et al. Nesprins, but not sun proteins, switch isoforms at the nuclear envelope during muscle development. *Dev Dyn*. 2010;239(3):998–1009.
16. Karczewski KJ, Francioli LC, Tiao G, et al.; Genome Aggregation Database Consortium. The mutational constraint spectrum quantified from variation in 141,456 humans. *Nature*. 2020; 581(7809):434–443.
17. Wiel L, Baakman C, Gilissen D, Veltman JA, Vriend G, Gilissen C. MetaDome: Pathogenicity analysis of genetic variants through aggregation of homologous human protein domains. *Hum Mutat*. 2019;40(8):1030–1038.
18. Leuzzi V, Rinna A, Gallucci M, et al. Ataxia, deafness, leukodystrophy: Inherited disorder of the white matter in three related patients. *Neurology*. 2000;54(12):2325–2328.
19. Lamond AI, Spector DL. Nuclear speckles: A model for nuclear organelles. *Nat Rev Mol Cell Biol*. 2003;4(8):605–612.
20. Rockel TD, Stuhlmann D, von Mikecz A. Proteasomes degrade proteins in focal subdomains of the human cell nucleus. *J Cell Sci*. 2005;118(Pt 22):5231–5242.
21. Lallemand-Breitenbach V, Zhu J, Puvion F, et al. Role of promyelocytic leukemia (PML) sumolation in nuclear body formation, 11S proteasome recruitment, and As2O3-induced PML or PML/retinoic acid receptor alpha degradation. *J Exp Med*. 2001;193(12):1361–1371.
22. Janer A, Martin E, Muriel MP, et al. PML clastosomes prevent nuclear accumulation of mutant ataxin-7 and other polyglutamine proteins. *J Cell Biol*. 2006;174(1):65–76.
23. Blank M. Targeted regulation of nuclear lamins by ubiquitin and ubiquitin-like modifiers. *Cells*. 2020;9(6):1340.
24. Dou Z, Xu C, Donahue G, et al. Autophagy mediates degradation of nuclear lamina. *Nature*. 2015;527(7576):105–109.
25. Melberg A, Hallberg L, Kalimo H, Raininko R. MR characteristics and neuropathology in adult-onset autosomal dominant leukodystrophy with autonomic symptoms. *AJNR Am J Neuroradiol*. 2006;27(4):904–911.
26. Ciechanover A. The unravelling of the ubiquitin system. *Nat Rev Mol Cell Biol*. 2015;16(5):322–324.
27. Rousseau A, Bertolotti A. Regulation of proteasome assembly and activity in health and disease. *Nat Rev Mol Cell Biol*. 2018; 19(11):697–19712.
28. Okamoto Y, Ozaki T, Miyazaki K, Aoyama M, Miyazaki M, Nakagawara A. UbcH10 is the cancer-related E2 ubiquitin-conjugating enzyme. *Cancer Res*. 2003;63(14):4167–4173.
29. Dhananjayan SC, Ismail A, Nawaz Z. Ubiquitin and control of transcription. *Essays Biochem*. 2005;41:69–80.
30. von Mikecz A. The nuclear ubiquitin-proteasome system. *J Cell Sci*. 2006;119(Pt 10):1977–1984.
31. Rotin D, Kumar S. Physiological functions of the HECT family of ubiquitin ligases. *Nat Rev Mol Cell Biol*. 2009;10(6):398–409.
32. Dechat T, Gesson K, Foisner R. Lamina-independent lamins in the nuclear interior serve important functions. *Cold Spring Harb Symp Quant Biol*. 2010;75:533–543.
33. Prokocimer M, Barkan R, Gruenbaum Y. Hutchinson-Gilford progeria syndrome through the lens of transcription. *Aging Cell*. 2013;12(4):533–543.
34. Moir RD, Spann TP, Herrmann H, Goldman RD. Disruption of nuclear lamin organization blocks the elongation phase of DNA replication. *J Cell Biol*. 2000;149(6):1179–1192.
35. Manju K, Muralikrishna B, Parnaik VK. Expression of disease-causing lamin A mutants impairs the formation of DNA repair foci. *J Cell Sci*. 2006;119(Pt 13):2704–2714.
36. Shimi T, Pfleghaar K, Kojima S, et al. The A- and B-type nuclear laminnetworks: Microdomains involved in chromatin organization and transcription. *Genes Dev*. 2008;22(24):3409–3421.
37. Dechat T, Adam SA, Goldman RD. Nuclear lamins and chromatin: When structure meets function. *Adv Enzyme Regul*. 2009; 49(1):157–166.
38. Brunet A, Forsberg F, Fan Q, Sæther T, Collas P. Nuclear lamin B1 interactions with chromatin during the circadian cycle are uncoupled from periodic gene expression. *Front Genet*. 2019;10: 917.
39. Earle AJ, Kirby TJ, Fedorchak GR, et al. Mutant lamins cause nuclear envelope rupture and DNA damage in skeletal muscle cells. *Nat Mater*. 2020;19(4):464–473.
40. Ulianov SV, Doronin SA, Khrameeva EE, et al. Nuclear lamina integrity is required for proper spatial organization of chromatin in Drosophila. *Nat Commun*. 2019;10(1):1176.

41. Vergnes L, Péterfy M, Bergo MO, Young SG, Reue K. Lamin B1 is required for mouse development and nuclear integrity. *Proc Natl Acad Sci U S A*. 2004;101(28):10428–10433.

42. Coffinier C, Jung HJ, Nobumori C, et al. Deficiencies in lamin B1 and lamin B2 cause neurodevelopmental defects and distinct nuclear shape abnormalities in neurons. *Mol Biol Cell*. 2011;22(23):4683–4693.

43. Lee JM, Tu Y, Tatar A, et al. Reciprocal knock-in mice to investigate the functional redundancy of lamin B1 and lamin B2. *Mol Biol Cell*. 2014;25(10):1666–1675.

44. Young SG, Jung HJ, Lee JM, Fong LG. Nuclear lamins and neurobiology. *Mol Cell Biol*. 2014;34(15):2776–2785.

45. Chen NY, Yang Y, Weston TA, et al. An absence of lamin B1 in migrating neurons causes nuclear membrane ruptures and cell death. *Proc Natl Acad Sci U S A*. 2019;116(51):25870–25879.

46. Brussino A, Vaula G, Cagnoli C, et al. A family with autosomal dominant leukodystrophy linked to 5q23.2-q23.3 without lamin B1 mutations. *Eur J Neurol*. 2010;17(4):541–549.

47. Barascu A, Le Chalony C, Pennarun G, et al. Oxidative stress induces an ATM-independent senescence pathway through p38 MAPK-mediated lamin B1 accumulation. *Embo J*. 2012;31(5):1080–1094.

48. Barascu A, Le Chalony C, Pennarun G, Genet D, Zaarour N, Bertrand P. Oxydative stress alters nuclear shape through lamins dysregulation: A route to senescence. *Nucleus*. 2012;3(5):411–417.

49. Molloy A, Cotter O, van Spaendonk R, Sistermans E, Sweeney B. A patient with a rare leukodystrophy related to lamin B1 duplication. *Ir Med J*. 2012;105(6):186–187.

50. Dai Y, Ma Y, Li S, et al. An LMNB1 duplication caused adult-onset autosomal dominant leukodystrophy in Chinese family: Clinical manifestations, neuroradiology and genetic diagnosis. *Front Mol Neurosci*. 2017;10:215.

51. Mezaki N, Miura T, Ogaki K, et al. Duplication and deletion upstream of LMNB1 in autosomal dominant adult-onset leukodystrophy. *Neurol Genet*. 2018;4(6):e292.

52. Pierce T, Worman HJ, Holy J. Neuronal differentiation of NT2/D1 teratocarcinoma cells is accompanied by a loss of lamin A/C expression and an increase in lamin B1 expression. *Exp Neurol*. 1999;157(2):241–250.

53. Lin ST, Fu YH. miR-23 regulation of lamin B1 is crucial for oligodendrocyte development and myelination. *Dis Model Mech*. 2009;2(3–4):178–188.

54. Lin ST, Huang Y, Zhang L, Heng MY, Ptáček LJ, Fu YH. MicroRNA-23a promotes myelination in the central nervous system. *Proc Natl Acad Sci U S A*. 2013;110(43):17468–17473.

55. Lin ST, Heng MY, Ptáček LJ, Fu YH. Regulation of myelination in the central nervous system by nuclear lamin B1 and non-coding RNAs. *Transl Neurodegener*. 2014;3(1):4.

56. Heng MY, Lin ST, Verret L, et al. Lamin B1 mediates cell-autonomous neuropathology in a leukodystrophy mouse model. *J Clin Invest*. 2013;123(6):2719–2729.

57. Rolyan H, Tyurina YY, Hernandez M, et al. Defects of lipid synthesis are linked to the age-dependent demyelination caused by lamin B1 overexpression. *J Neurosci*. 2015;35(34):12002–11217.

58. Giacomini C, Mahajani S, Ruffilli R, Marotta R, Gasparini L. Lamin B1 protein is required for dendrite development in primary mouse cortical neurons. *Mol Biol Cell*. 2016;27(1):35–47.

59. Yattah C, Hernandez M, Huang D, Park H, Liao W, Casaccia P. Dynamic lamin B1-gene association during oligodendrocyte progenitor differentiation. *Neurochem Res*. 2020;45(3):606–619.

60. Takamori Y, Tamura Y, Kataoka Y, et al. Differential expression of nuclear lamin, the major component of nuclear lamina, during neurogenesis in two germinal regions of adult rat brain. *Eur J Neurosci*. 2007;25(6):1653.

61. Mahajani S, Giacomini C, Marinaro F, De Pietri D, Tonelli D, Contestabile A. Lamin B1 levels modulate differentiation into neurons during embryonic corticogenesis. *Sci Rep*. 2017;7(1):4897.

62. Khanna R, Krishnamoorthy V, Parnaik VK. E3 ubiquitin ligase RNF123 targets lamin B1 and lamin-binding proteins. *Febs J*. 2018;285(12):2243–2262.

63. Krishnamoorthy V, Khanna R, Parnaik VK. E3 ubiquitin ligase HECW2 targets PCNA and lamin B1. *Biochim Biophys Acta Mol Cell Res*. 2018;1865(8):1088–1104.

64. Zhen R, Moo C, Zhao Z, et al. Wdr26 regulates nuclear condensation in developing erythroblasts. *Blood*. 2020;135(3):208–219.

65. Peretto G, Di Resta C, Perversi J, et al.; Italian Network for Laminopathies (NIL). Cardiac and neuromuscular features of patients with LMNA-related cardiomyopathy. *Ann Intern Med*. 2019;171(7):458–463.

66. Crasto S, My I, Di PE. The broad spectrum of LMNA cardiac diseases: From molecular mechanisms to clinical phenotype. *Front Physiol*. 2020;11:761.

67. Sheikh FN, Hassan SA, Alam D, Kundi M, Hassan M. Lamin A/C cardiomyopathy with E203K pathogenic mutation. *Cureus*. 2020;12:e7761.

68. Lattanzi G, Maggi L, Araujo-Vilar D. Laminopathies. *Nucleus*. 2018;9(1):543–544.

69. Muchir A, Massart C, van Engelen BG, Lammens M, Bonne G, Worman HJ. Proteasome-mediated degradation of integral inner nuclear membrane protein emerin in fibroblasts lacking A-type lamins. *Biochem Biophys Res Commun*. 2006;351(4):1011–1017.

70. Chaturvedi P, Parnaik VK. Lamin A rod domain mutants target heterochromatin protein 1alpha and beta for proteasomal degradation by activation of F-box protein, FBXW10. *PLoS One*. 2010;5(5):e10620.

71. Parnaik VK, Chaturvedi P, Muralikrishna B. Lamins, laminopathies and disease mechanisms: Possible role for proteasomal degradation of key regulatory proteins. *J Biosci*. 2011;36(3):471–479.

72. Johnson BR, Nitta RT, Frock RL, et al. A-type lamins regulate retinoblastoma protein function by promoting subnuclear localization and preventing proteasomal degradation. *Proc Natl Acad Sci U S A*. 2004;101(26):9677–9682.

73. Chaturvedi P, Khanna R, Parnaik VK. Ubiquitin ligase RNF123 mediates degradation of heterochromatin protein 1α and β in lamin A/C knock-down cells. *PLoS One*. 2012;7(10):e47558

74. Buchwalter A, Schulte R, Tsai H, Capitanio J, Hetzer M. Selective clearance of the inner nuclear membrane protein emerin by vesicular transport during ER stress. *Elife*. 2019;8:e49796

75. Koch B, Yu HG. Regulation of inner nuclear membrane associated protein degradation. *Nucleus*. 2019;10(1):169–180.

76. Muralikrishna B, Chaturvedi P, Sinha K, Parnaik VK. Lamin misexpression upregulates three distinct ubiquitin ligase systems that degrade ATR kinase in HeLa cells. *Mol Cell Biochem*. 2012;365(1–2):323–332.

77. Horn HF, Brownstein Z, Lenz DR, et al. The LINC complex is essential for hearing. *J Clin Invest*. 2013;123(2):740–750.

78. Masterson J, Yıldırım B, Gökkaya E, Tokgöz Yılmaz S, Tekin M. A novel variant in SYNE4 confirms its causative role in sensorineural hearing loss. *Balkan Med J*. 2018;35(2):196–198.

79. Tan KL, Haelterman NA, Kwartler CS, et al.; University of Washington Center for Mendelian Genomics. Ari-1 regulates myonuclear organization together with Parkin and is associated with aortic aneurysms. *Dev Cell*. 2018;45(2):226–244.e8.